Subglacial channels, climate warming, and increasing frequency of Alpine glacier snout collapse

Pascal E. Egli[1*], Bruno Belotti[2], Boris Ouvry[3], James Irving[4], Stuart N. Lane[1]
[1] Institute of Earth Surface Dynamics, University of Lausanne, Switzerland
[2] Department of Geological Sciences, University of Idaho, Idaho, USA
[3] Institute of Geography, University of Zurich, Switzerland
[4] Institute of Earth Sciences, University of Lausanne, Switzerland
Corresponding author: Pascal Egli (eglipascal@gmx.net)

Key Points:

- A survey of 22 Alpine glaciers shows increased margin collapse frequency linked to rapid climate warming since the 1980s
- Collapse appears to be associated with glacier thinning, stagnation of snout margins and reduced rates of subglacial channel closure
- Glaciers with collapse features have retreat rates that are more sensitive to inter-annual temperature fluctuations
- Intensive study of a collapse event confirms that significant up-glacier extension of an unpressurised subglacial channel drives the collapse process

Abstract

Alpine glacier retreat has increased markedly since the late 1980s, and is commonly linked to the effects of rising temperature on surface melt. Less considered are processes associated with glacier surface collapse. A survey of 22 retreating Swiss glaciers suggests that snout marginal collapse events have increased in frequency since the late 1980s, driven by ice thinning and reductions in glacier-longitudinal ice flux. Detailed measurement of a collapse event at one glacier showed vertical deformation of the surface above the main subglacial channel. But with low rates of longitudinal flux and vertical creep closure, this was insufficient to close the channel in the snout marginal zone. We hypothesise that this maintains contact between subglacial ice and the atmosphere, allowing greater incursion of warm air up-glacier, thus enhancing melt from below. The associated enlargening of subglacial channels at glacier snouts leads to surface collapse and removal of ice via fluvial processes.

Plain language summary

Mountain glaciers have been melting and retreating more rapidly since the onset of accelerated atmospheric warming in the late 1980s. Our study examines 22 Swiss glaciers in order to understand why for some glaciers the ice surface close to the glacier margin breaks down and forms collapse features, and for others it does not. We find that the combination of thin ice having a low surface slope results in locally reduced ice flow, which causes subglacial channels to close more slowly and eventually leads to channel roof collapse. A detailed study based on ground-penetrating radar and drone surveys at one of the glaciers showed that the subglacial channel there is very wide and shallow, and that its strongly sinuous shape may have contributed to a recent ice-surface collapse. Ice blocks from the melting and collapsing channel were flushed out by the proglacial stream. We observe that such collapse features have become more frequent with a stronger increase in air temperature. Visibly, such collapse features may contribute to more rapid glacier recession.

1 Introduction

Alpine glaciers have been retreating rapidly since the 1980s because of rapid climate warming (Salzmann et al., 2012; Huss et al., 2010; Paul & Haeberli, 2008). Retreat is forecast to accelerate in the coming decades (Zekollari et al., 2019). The primary mechanism of mass loss is surface melt. However, other mechanisms may play an important role. One of these involves the collapse of subglacial channels in the snout marginal zone, driven by thinning ice combined with slow creep closure. After collapse, the ice is removed via the channel to the glacier outlet. This mechanism of glacier retreat was first described some time ago as 'subglacial stoping' or 'block caving' (Paige, 1956; Loewe, 1957).

There are few examples where such collapse behaviour has been documented and quantified (Bartholomaus et al., 2011; Dewald et al., 2021; Kellerer-Pirklbauer & Kulmer, 2018; Konrad, 1998; Lindström, 1993; Stocker-Waldhuber et al., 2017). As a result, little is known about where and when these collapse features form and whether or not their frequency of formation is changing in response to climate warming.
We hypothesise that the formation of collapse features is driven by three interconnected mechanisms: (1) high temperatures lead to high melt rates and shallow ice in the snout marginal area of glaciers; (2) shallow ice means reduced longitudinal ice flow velocities and reduced creep closure of subglacial channels; and (3) the presence of a subglacial channel underneath shallow ice can initiate a collapse feature due to upwards melting and block caving.

In this study, we perform statistical analysis on a sample of 22 Swiss glaciers based on 24 glacier properties, climate data, and historical aerial imagery in order to investigate how pervasive these collapse events are becoming and to test the abovementioned hypotheses. The results obtained are supported by the intensive study of one retreating glacier which experienced a recent (2017-2018) collapse event, the Glacier d'Otemma. For this glacier we were able to measure ablation, surface elevation change, and the position of the corresponding subglacial channel, which allowed us to document the processes leading to the channel collapse.

2 Materials and Methods

2.1 Overview

We first examine the conditions driving snout margin collapse through the analysis of topography, ice thickness, historical aerial imagery, air temperature, and glacier retreat data for 22 glaciers in the western and central Swiss Alps (Figure S1). We focus on Swiss glaciers because of the widespread availability of measurements, notably of glacier bed topography, ice thickness, and aerial imagery, that allow us to build an extensive database of the conditions at glacier snout margins. Based on historical and contemporary aerial imagery, 12 glaciers were selected that were found to show at least one subglacial channel collapse feature near their terminus since the first date of aerial imagery in 1938. In addition, 10 glaciers not exhibiting collapse features were chosen, all of them located in close vicinity to the aforementioned glaciers and having comparable topography and size to nearby glaciers with collapse features, in order to do a balanced statistical comparison (Figure S1).

In the second part of our study, we examine in detail the ice surface lowering, subglacial channel position, and ice ablation measured using uncrewed aerial vehicle (UAV) imagery, ground-penetrating radar (GPR) measurements, and ablation stakes, respectively, before and during a collapse event at the Glacier d'Otemma (2017-2018). This is done to investigate the mechanisms leading to such events and to reveal the exent to which unpressurised subglacial marginal channels can extend up-glacier.

2.2 Frequency of collapse events

To test whether the frequency of snout marginal channel collapse events is increasing with time, we used the SwissTopo LUBIS visualization system. LUBIS contains all of the digitized aerial imagery held by SwissTopo back to 1938. We inspected the imagery available for the snout region of each glacier in order to determine whether or not a collapse feature was present (Figure S1). Each instance where the snout of one of the glaciers was shown was counted as an observation. On some aerial images several of the chosen glacier snouts were visible, meaning that the same image could be counted more than once. There were 179 observations in total, of which 29 showed a collapse feature and 150 did not. After eliminating multiple counts of the same collapse feature, 27 separate collapse events remained. The cumulative number of identified collapses through time is presented alongside the cumulative number of observations made in order to account for a change in the number of observations after 1980.

2.3 Characterization of collapse conditions

For each of the 22 glaciers considered, we assembled a database consisting of (i) surface elevation information from the SwissAlti3D Digital Elevation Model (SwissTopo, 2020); (ii) bed topography and ice thickness measurements based on GPR data and modelling (Grab et al., 2021); and (iii) retreat history information from the Swiss Glacier Monitoring Network (GLAMOS, 1885-2019). Supporting Information section 3.1 explains how this database was put together and Table S2 lists the 24 properties, considered in our analysis, that were derived from the data either directly (e.g., ice thickness in the snout marginal zone) or inferred from basic process laws (e.g., mean snout marginal glacier velocity).

To investigate the extent to which glaciers showing collapse features are likely to have lower longitudinal ice flux and subglacial channel closure, we determined the mean ice thickness, bed slope and surface slope for the entire glacier and for the first 2 km of

each glacier tongue. These parameters were also determined for a 100 m radius around each of the most recent collapse zone locations. The mean distance between the center of the most recent collapse feature and the glacier terminus for the 12 glaciers showing collapse features was found to be ~250 m. Thus, for glaciers not showing collapse features, a hypothetical collapse zone of 100 m radius, positioned at the centerline at a horizontal distance of 250 m from the terminus, was used. Supporting Information section 3.1 explains how the latter information was used to estimate the mean longitudinal velocity and vertical closure rate.

We also characterized glacier retreat using GLAMOS (GLAMOS, 1881-2019) data to determine length change and variability in length change since 1987, which is the date considered for the onset of rapid recession related to climate warming in the study region (Costa et al., 2018).

Finally, Jarque and Bera (1980) tests of the 22 samples of each property in Table S2 suggested that 13 out of 24 properties were non-Gaussian distributed at the 5% significance level. Consequently, we used Mann and Whitney (1947) U tests to assess the extent to which these properties differed between those glaciers showing channel collapse and those not showing collapse.

2.4 Relationship between summer air temperatures and retreat

If collapse formation is driven by the incursion of warm air underneath snout margins via unpressurised subglacial channels, then we might expect variation in the annual snout recession to be more sensitive to mean annual summer air temperature variations than for those glaciers where snout recession is driven by temperature effects on surface melt alone. To investigate this hypothesis, we identified for each glacier the year of onset of continuous retreat according to the GLAMOS (1881-2019) database (Supporting Information section 3.7). We then calculated a time-series of annual retreat rate (R_A) and its mean (R_M) for each glacier for the period during which each glacier was retreating. For the same period, we determined the annual mean summer air temperature in the snout region (T_{SA}) and its mean (T_{SM}). This was done using spatially

interpolated and gridded MeteoSwiss data (temperature 2 m above the ground between June 1 and August 31) from the center of the 1x1 km grid cell located closest to the glacier terminus. We determined the coefficient of variation of retreat (R_{CV}) by dividing the standard deviation of retreat by the mean annual retreat rate. We computed the Pearson's correlation coefficient (P_{RT}) between T_{SA} *and* R_A and we calculated the sensitivity of R_A to T_{SA} (S_{RT}) using simple linear regression. For each of these parameters a Jarque and Bera (1980) test was used to check for normality (H_o, normal distribution, could not be rejected at p=0.05). This allowed us to compare glaciers with and without collapse features using Student's t, for all parameters except S_{RT}. The latter was not normally distributed (p<0.05) and so we used the Mann and Whitney (1947) U test.

2.5 Surface dynamics and subglacial channel collapse at the Glacier d'Otemma

To establish in more detail the physical processes that explain these extensive inferences, we studied the process of snout marginal collapse for one of the glaciers in the database, the Glacier d'Otemma (Figure S1). In 2018, this glacier had a snout elevation of 2490 m and a maximum elevation of 3600 m. A collapse feature was observed to be forming 210 m upstream of the glacier snout in 2017, where the glacier surface slope was 10°, the glacier bed slope was 12°, and the mean ice thickness was 22 m. The collapse feature coincided with a major subglacial channel that became visible after the collapse event in 2018. We aimed to determine the planform geometry of the subglacial channel and vertical ice deformation of the snout zone.

To determine the planform geometry of the subglacial channel, during the summer of 2017, we acquired a series of densely spaced GPR lines over the snout zone of the Glacier d'Otemma that provided us with high-resolution images of the main subglacial channel location (Egli et al., 2021). The channel outline in the northeast is based on an additional GPR dataset, processed in the exact same way as in Egli et al. (2021). We also calculated the Shreve hydraulic potential (Shreve, 1972;, Figure S14; section 3.2 in Supporting Information).

We hypothesize that if the subglacial channel close to the glacier snout was unpressurised and large enough, then we might see greater rates of vertical deformation on the ice surface in this location due to creep, albeit insufficient to close the channel, thereby setting the preconditions for a subglacial channel collapse feature and at the same time providing a diagnostic tool of the spatial extent of unpressurised channels. Thus, to calculate vertical ice deformation, UAV surveys were undertaken for the purpose of structure from motion multi-view stereo (SfM-MVS) photogrammetry (Supporting Information section 3.2, Figures S3, S4, S5). These also allowed us to visualise the development of a collapse feature (Figure S15). We used two surveys to determine vertical deformation on the 7th of August 2018 and on the 23rd of August 2018 whilst the collapse was happening. Each involved ~1000 images and was supported by 54 ground control points (GCPs) that were surveyed using a differential global positioning system (dGPS). Digital elevation models (DEMs) were produced applying a standard processing workflow (James et al., 2020; Rossini et al., 2018, Gindraux et al., 2017; Westoby et al., 2012; Supporting Information section 2.2; Figure S3) using the Agisoft Metashape© software. A DEM of difference (DoD; dz_{net}) showing the difference in surface elevation between the two surveys (16 days apart) was then computed. We did not correct the surface elevation change for lateral ice flux as the lateral velocity in the snout margin was measured by dGPS at the ablation stakes as only a few centimeters per month.

In order to distinguish between ablation and ice dynamics, we defined the net surface height change (dz_{net}), as the sum of a component due to vertical deformation ($dz_{dynamics}$) and a component due to ablation ($dz_{ablation}$):

$$dz_{net} = dz_{dynamics} + dz_{ablation} \quad [1]$$

The ablation component ($dz_{ablation}$) was estimated from manual measurement of melt for 49 stakes distributed across the area. These measurements were interpolated spatially using kriging to yield $dz_{ablation}$. The latter was substracted from d_{znet} to derive the surface change due to ice dynamics, $dz_{dynamics}$ (Supporting Information section 3.3).

To test for the influence of variables such as aspect, reflectance, slope or debris cover on ice surface elevation change and melt we computed their correlations with dz_{net} and $dz_{ablation}$ (Figure S7, S8, Table S4). As a proxy for the albedo we looked at surface reflectance as a measure for the fraction of short wave radiation reflected (Rippin et al., 2015).

Finally, we tested for a relationship between the presence of a subglacial channel and patterns of increased ice surface elevation change. Based on the GPR-derived channel outlines and on the Shreve hydraulic potential (Figure S14), the ablation stakes were classified according to the likelihood that they were located on top of a subglacial channel in order to assess the importance of the presence of a subglacial channel for ice surface lowering (Supporting Information section 3.8; Figure 3a-d).

3 Results

3.1 Collapse events and their changing frequency

Figure 1 shows the most recent channel collapse features identified in aerial imagery for the different glaciers considered. They differ in the detail of their form, but most have concentric crevasse-like features present in both the early stages of development (e.g. Figure 1c, 1i), during collapse (e.g. Figure 1a) and afterwards (e.g. Figure 1e, 1j). The images confirm that these features can develop in both debris-free and debris-covered snout marginal zones.

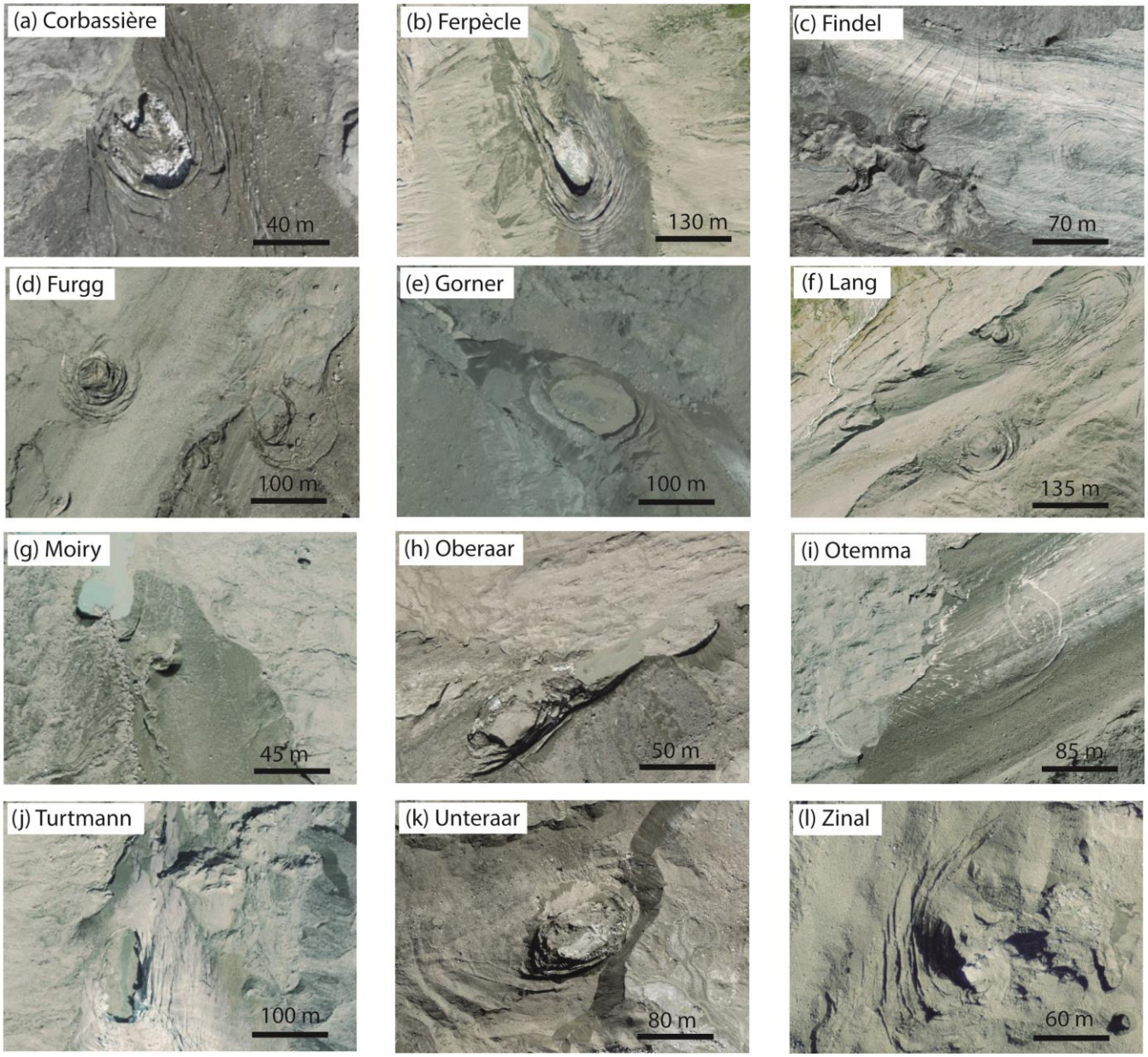

Figure 1: *Composite image of aerial imagery of collapse features. (a) Glacier de Corbassière (2020, partly debris covered), (b) Glacier de Ferpècle (2016, partly debris covered), (c) Findelengletscher (2017, debris free), (d), Furgggletscher (2019, largely debris covered), (e) Gornergletscher (2006, partly debris covered), (f) Langgletscher (2017, largely debris covered), (g) Glacier de Moiry (2017, partly debris covered), (h) Oberaargletscher (2018, largely debris covered), (i) Glacier d'Otemma (2017, partly debris covered), (j) Turtmanngletscher (2017, debris free), (k) Unteraargletscher (2018, largely debris covered), (l) Glacier de Zinal (2016, largely debris covered)*

Figure 2 shows the cumulative number of different collapse events observed on the aerial images, along with the cumulative number of observations, as a function of time from 1938 to present. The 5-year running average and standard deviation of the mean summer air temperature of all glaciers with collapse features are also displayed for comparison. We see that, as described previously, there is an increase in the frequency of observations starting in the early 1980s. Interestingly, however, the frequency of observed collapse events only starts to increase after the year 2000. Specifically, from the mid to late 1990s there is a substantial increase in the frequency of collapse events, and especially in the last 5 years, suggesting that as climate warming accelerates and as glacier retreat continues, so does the tendency for collapse features to form.

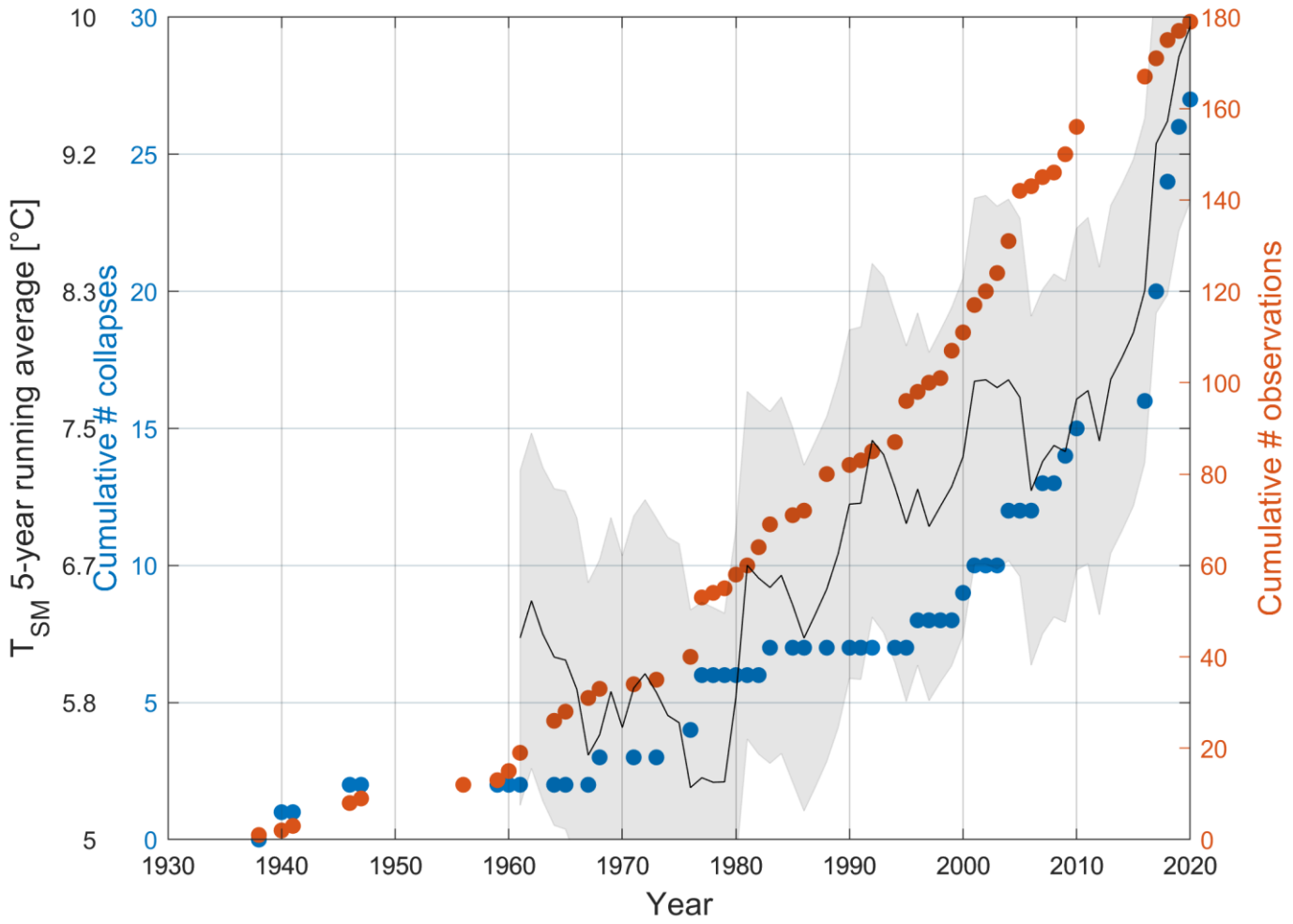

***Figure 2**: Cumulative number of collapse events (blue dots) and cumulative number of observations (orange dots) since 1938 for all 22 glaciers considered in our study. 5-year running average of the mean summer temperature (T_{SM}, black line) since 1961 over the 12 glaciers exhibiting one or several collapse events, along with the standard deviation around the mean temperature (grey shaded area).*

3.2 Statistical analysis of collapse conditions

Application of the Mann-Whitney U test with a 5% - 95% confidence interval to all 24 properties (Table S2) shows that the collapse and non-collapse groups of glaciers only differ significantly with respect to five variables (Figure S2); (1) ice thickness near the collapse area (Figure S2a): (2) estimated creep closure rate in the collapse area (Figure S2b); (3) estimated ice flow velocity in the collapse area (Figure S2c); (4) the mean surface slope within the collapse area (Figure S2d); and (5) the mean surface slope as measured from the upstream edge to the downstream edge of the collapse area (Figure S2e). These results suggest that relatively thin ice, a shallow surface slope and, a function of these two parameters, low longitudinal flow velocity in the immediate vicinity of a marginal subglacial channel are the conditions required for collapse. Ice having a thickness of less than 50 m, for example, results in creep closure being small enough that a subglacial channel with a diameter of 5 m does not close over winter (calculations according to Supporting Information section 3.1; results for each glacier in Table S6). Combined with a small surface slope (a median of 11.4° for glaciers with collapse features; Table S6) and a small bed slope (a median of 14.3° for glaciers with collapse features; Table S6) this shallow ice also results in very low estimated glacier-longitudinal flux, further impeding channel closure. Retreat and ice thickness data are

displayed in Table S3 (further details are provided in Table S5), whereas the results of the Mann-Whitney U test are displayed in Table S2.

3.3 Relationship between summer air temperatures and retreat

The mean annual retreat rate, the mean summer temperature in the snout zone in the period during which each glacier was retreating, and the coefficient of variation of retreat did not differ between glaciers exhibiting and not exhibiting collapse features. However, glaciers with collapse features had systematically more negative correlations between annual retreat and mean annual summer temperature ($p<0.05$) and significantly higher sensitivity of annual variations in glacier length to mean annual summer temperature ($p<0.05$) (Figure S11). For the glaciers with collapse features, 6 out of 12 had significant ($p<0.05$) negative P_{RT} values compared with 2 out of 10 non-collapse glaciers. Thus, a diagnostic feature of glaciers showing collapse features appears to be a stronger sensitivity to mean summer temperature.

3.4 Measurement of an active collapse at the Glacier d'Otemma

Figure 3a shows the UAV-based orthoimage of the Glacier d'Otemma that was taken on August 7, 2018, upon which are superposed the positions of the ablation stakes and the location of a 10-m-wide subglacial channel that was detected based on high-resolution GPR data acquired a year earlier in August 2017 (Egli et al., 2021). The orthoimage shows development of a collapse feature close to the snout of the glacier near the downstream end of the identified channel.

Figure 3b shows the surface elevation changes that occurred between August 7 and 23, 2018. General surface height loss is observed all along the glacier tongue. This loss is greatest (up to 1.2 m) in areas of bare ice and reduced where there is higher debris cover (Figures 3a and 3b). Figure 3b also shows increased lowering of the surface above the GPR-identified subglacial channel. Areas outside of the glacier outline show little

348 vertical change, with the exception for zones where 'dead ice' is melting under the debris
349 cover (e.g. at 200 m / 280 m relative Easting / Northing in Figure 3b). Figure 3c shows
350 the surface change after removal of the kriging-interpolated ablation stake
351 measurements. This results in some differences from the original DoD, but the pattern
352 of strong surface lowering in the vicinity of the subglacial channel persists. To rule out
353 factors other than the presence of a subglacial channel that may cause surface elevation
354 changes, we examined the correlations between surface change and the glacier surface
355 slope, reflectance, aspect and elevation for small patches (0.5 x 0.5 m) around each
356 ablation stake location. None of these four variables were correlated with elevation
357 change or ablation rate (Table S4, Figures S7 and S8). Thus, the surface change shown
358 in Figure 3c can be attributed to enhanced vertical deformation related to the presence
359 of a subglacial channel that must have been at atmospheric pressure; but where this
360 enhanced deformation was not sufficient for the channel to close and to become
361 pressurised.
362
363 Surface elevation changes and ablation measurements were compared for three
364 different categories defined according to position: locations known to be above the
365 identified subglacial channel (called on-channel), locations that are likely to be above
366 the channel (called likely on-channel), and locations that are off-channel (called off-
367 channel). A Mann-Whitney U test shows no significant difference (p=0.05) in ablation
368 between on-channel/likely-on and off-channel locations. With regard to surface
369 elevation changes, on the other hand, the Mann-Whitney U test shows that on-channel
370 values are significantly different from those at off channel stakes ($p<0.05$), whereas
371 likely on-channel values are not significantly different from off-channel values (Figure
372 S12, Table S5).
373

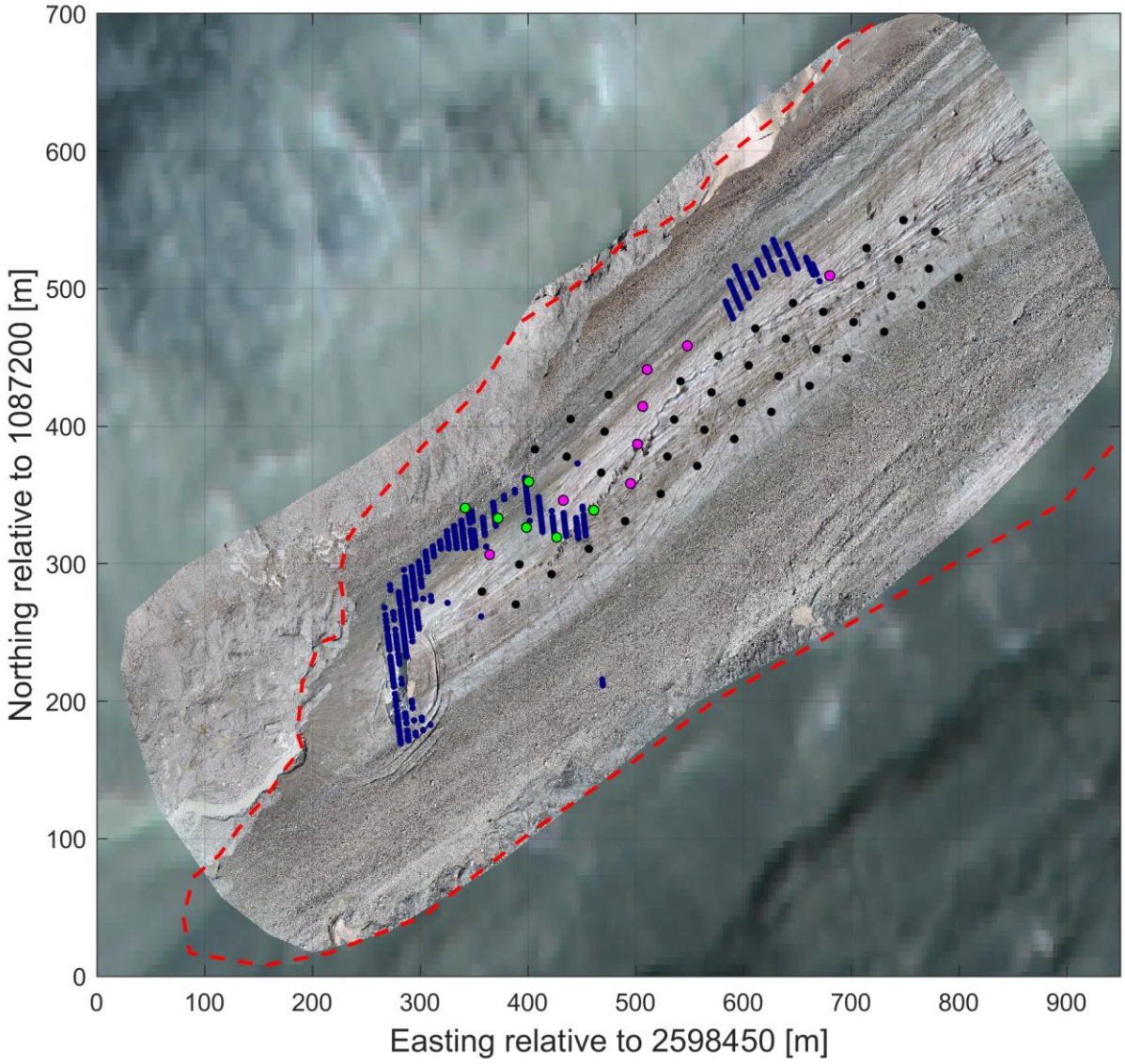
Northing relative to 1087200 [m]
Easting relative to 2598450 [m]
0
100
200
300
400
500
600
700
800
900

(a)

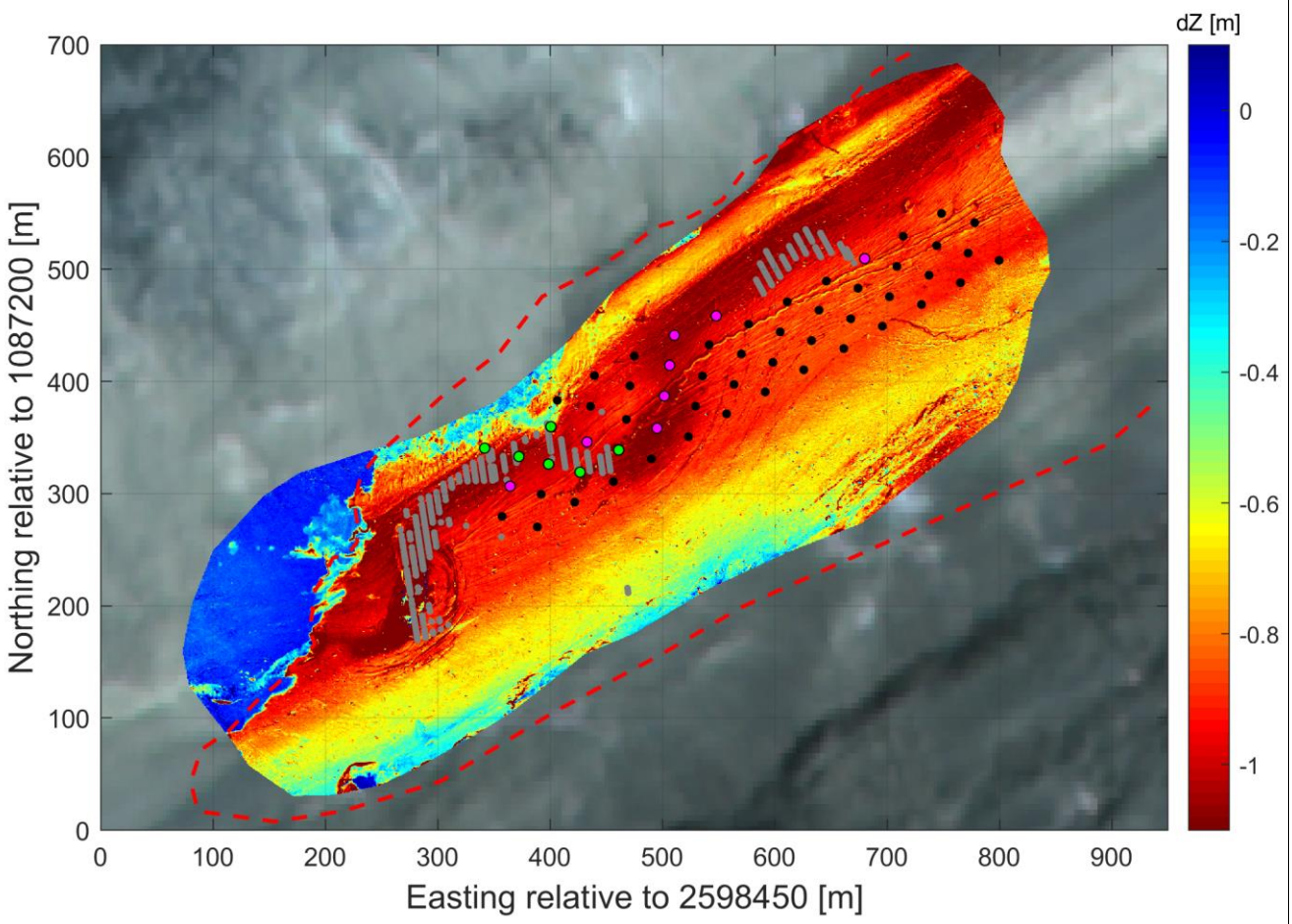
dZ [m]
0
-0.2
-0.4
-0.6
-0.8
-1
Northing relative to 1087200 [m]
0
100
200
300
400
500
600
700
Easting relative to 2598450 [m]
0
100
200
300
400
500
600
700
800
900

(b)

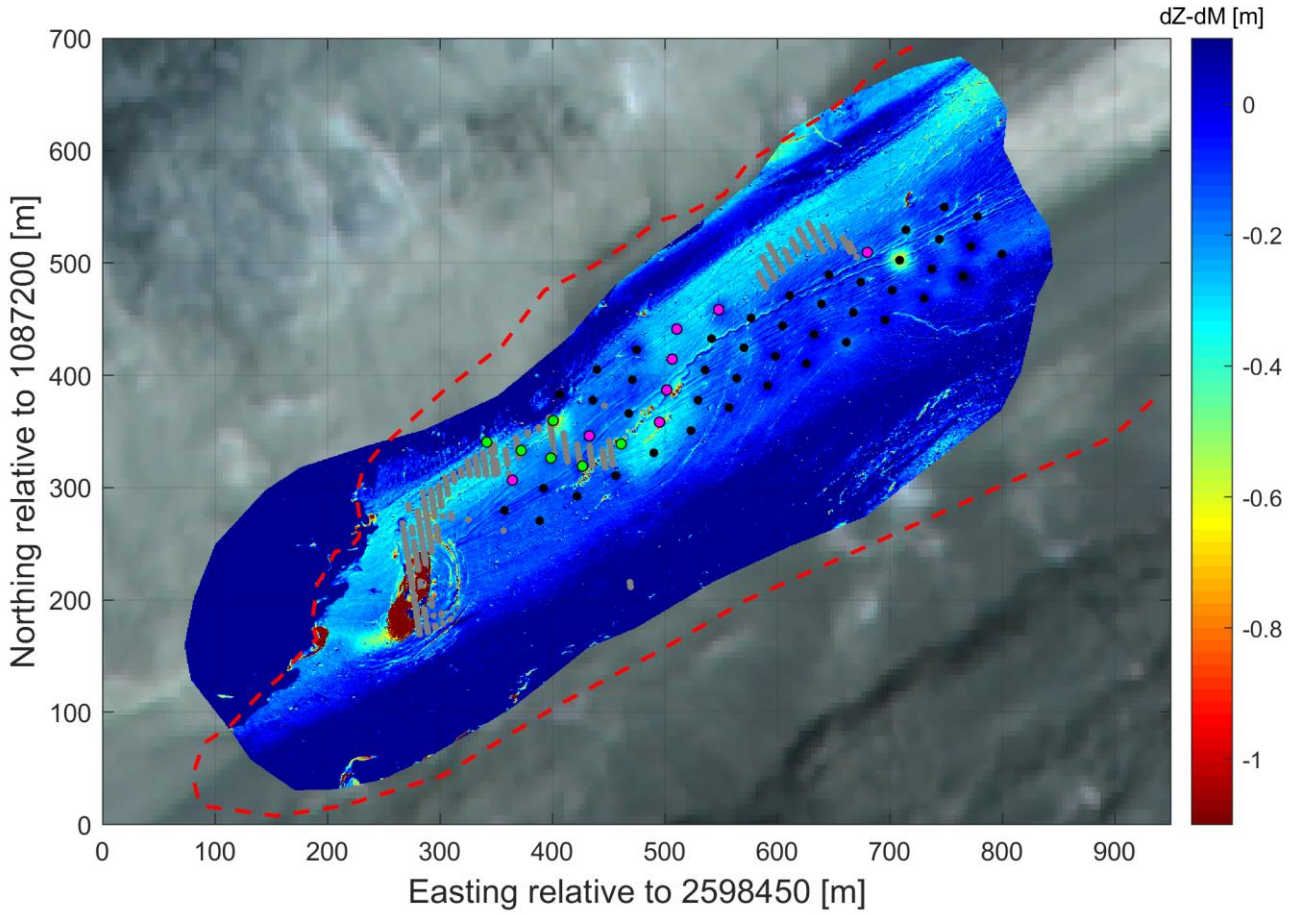
dZ-dM [m]
0
-0.2
-0.4
-0.6
-0.8
-1
Northing relative to 1087200 [m]
0
100
200
300
400
500
600
700
Easting relative to 2598450 [m]
0
100
200
300
400
500
600
700
800
900

(c)

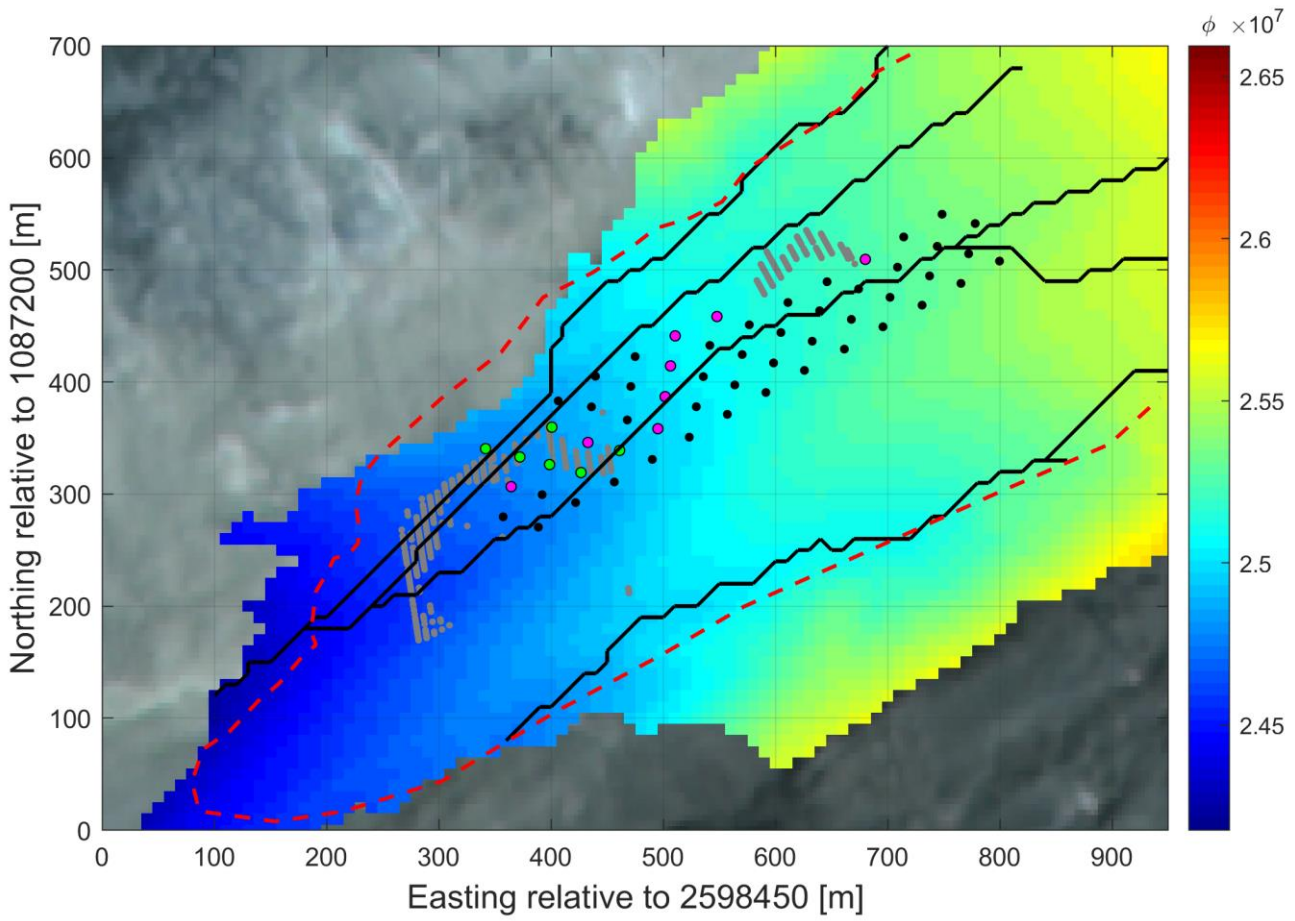

(d)

Figure 3*: (a) Orthophoto with locations of ablation stakes (dots) and subglacial channel locations in blue stipples (b) Change in surface elevation (DoD) computed between August 7 and 23, 2018, overlain by subglacial channel positions (grey stipples) detected based on GPR data from August 2017 (Egli et al., 2021). The collapsed area is clearly visible at 280 m Easting / 200 m Northing. (c) Image in (b) after subtraction of ablation measurements. The ablation stakes are subdivided in*

different colors, where black is for stakes located off-channel, cyan is for stakes located almost certainly on top of a subglacial channel (on-channel) and magenta is for stakes likely to be located on-channel, according to a map of the Shreve potential (Figure 6d) and to the proximity to the GPR-derived channels. Ablation was interpolated using kriging in order to fit the grid cells of the DEMs. There are some obvious local artifacts such as the point at 700 m Easting / 500 m Northing, but the strong ablation pattern from the image in (b) is preserved.

4 Interpretation and discussion

The analysis of historical imagery has revealed a systematic increase in the frequency of surface collapse features due to 'subglacial stoping' or 'block caving' (Loewe, 1957; Paige, 1956) in a set of Swiss glaciers since the mid to late 1990s (Figure 2) and about 5 to 10 years after the onset of rapid climate warming for this region (Costa et al., 2018). Such a delay is not surprising as most Alpine glaciers show a lag in the onset of retreat following a reduction in accumulation and an increase in ablation (Jouvet et al., 2011). Although the examined glaciers differ significantly in properties such as size, elevation range, and retreat rate, collapse features shown in Figure 1 were found predominantly in those glaciers having margins comprised of thin ice (generally with a thickness of less than 50 m; Table S3) and with shallow surface slopes and bed slopes (both less than 23°; Table S6). Flow velocity calculations suggested that these were zones of almost no longitudinal ice flux (Figure S2c, S2d) and reduced vertical channel closure rates (Figure S2b).

Intensive investigation of one of the 12 glaciers with collapse features showed that the collapse was centered directly over a subglacial channel. Remarkably, enhanced vertical deformation was observed above this channel for at least 600 m up glacier (Figure 3b, 3c) Any void under a glacier should be subject to void-directed ice flow unless the water pressure in the void equals the ice overburden pressure (Nye, 1953; Fountain and Walder, 1998). The enhanced vertical deformation observed above the subglacial channel at Otemma indicates that the latter was not the case for some way up-glacier.

Indeed, it is likely that this channel was at atmospheric pressure but that the vertical deformation was not enough to close the void. Based on the analysis presented in Hooke (1984, Figure 2) and with the thickness of ice at the snout of the glacier and a glacier bed slope that is marginally greater than the glacier surface slope, the channel is likely to be open. Our work importantly suggests that locally-increased vertical deformation rates on Alpine glaciers may be used to map the position of such subglacial channels flowing at atmospheric pressure.

The vertical deformation over the subglacial channel at the Glacier d'Otemma was approximately 0.2 to 0.3 m over a 16 day period (Figure 3c). Theoretical calculations using Hooke (1984) (Supplementary Information section 3.1) for the glacier suggested a closure of 0.18 m per year if we assume a 5-m diameter semi-circular channel. One explanation for a higher closure rate than predicted by the theory is that the channel is wider and flatter than an assumed semi-circle, as has now been observed in boreholes at the Glacier d'Otemma in summer 2021, and reported for Rhonegletscher (Church et al., 2021). The analysis using the theory on shallow subglacial conduits by Hooke et al. (1990) produces closure rate estimates over a 16-day period of ~0.03 to 0.13 m (Supplementary Information section 3.5).

These theoretical estimates are much closer to, albeit still lower than, the measured vertical deformation rate. The question then becomes why is it possible to maintain such high vertical deformation rates without returning the subglacial channel to a pressurized state? Field observations revealed large blocks of ice in the braid plain downstream from the glacier during the collapse event. We propose that as the ice overlying the subglacial channel close to the terminus is thin (~5-7 m; Figure S13 in Supporting Information) and as it creeps towards the channel, ice blocks may fall off the ceiling (block caving; Paige, 1956). Thus, whilst there is an enhanced vertical deformation rate additional ice is lost via subglacial caving rather than contributing to subglacial channel closure. These findings are supported by the results of a study of more than 1400 Esker enlargements assumed to indicate ice marginal subglacial channel collapse in the late stage of rapid ice sheet retreat (Dewald et al., 2021).

There are two additional mechanisms that may play a role in the development of collapse features and that merit further investigation. The first relates to the greater sensitivity in the retreat of glaciers with collapse features to inter-annual summer temperature variation (Figure S11b). This sensitivity could arise from reduced longitudinal flux in the snout margin of such glaciers (Figure S2c), but it could also arise because of enhanced subglacial exposure to warm air during summers. The measured vertical deformation at the Glacier d'Otemma suggests a significant up-glacier extent of water flow at atmospheric pressure (Figure 3b and 3c) and hence subglacial exposure to the atmosphere and warm air incursion.

The second mechanism to note is suggested in Figure 3a, which shows that the subglacial channel at the Glacier d'Otemma is meandering and that the collapse feature forms at a bend in the channel.

The time-series images of collapse at the Otemma glacier shows that the collapse morphology has meander-parallel crevasses (Figure S15). The possibility that subglacial channels are sinuous has been recognized, notably in studies of dye breakout curves (Kohler, 1995) suggesting the presence of open-channel flow with walls comprised of ice and/or till that can be mechanically eroded. It is well-established that straight rivers that are able to erode their beds and/or banks tend to initiate meandering as a result of the inherent instability related to the effects of turbulent anisotropy on secondary circulation and which tends to grow as a function of time across a wide range of river scales (Dey and Ali, 2017). In theory, deviation from a glacier-longitudinal orientation exposes the channel to greater longitudinal fluxes and hence greater closure so meaning that subglacial channels can't meander unless they can erode into bedrock. The margins of temperate Alpine glaciers are commonly zones of ice compression (Hart, 1995) as a zone of colder surface ice in the ablation zone connects with the bed at the snout margin (Moore et al., 2009). This would also aid closure of non-longitudinally-oriented channels. At the Otemma glacier with the estimated longitudinal velocities (1.29 m per year, Table S4) the 10-m-wide subglacial channel would only close by around 10 to 15% per year. This would allow maintenance of channels that meander. Thus, as glaciers thin and their loingitudinal velocities fall, not only do subglacial channels close less readily, they may

be increasingly able to maintain a meandering form. As technologies for mapping subglacial channels improve, it should become possible to test the hypothesis that the formation of meandering open channel flow under glacier snout margins with low longitudinal ice flux is a contributory mechanism to the onset of collapse.

Our wider statistical analysis suggests that glaciers with collapse features tend to have lower rates of longitudinal flux and so reduced compression and longitudinal closure (Figure S2f). Low longitudinal flux is a consequence of short-term increases in ablation and glacier thinning and long-term reduction of flux of accumulated ice into the ablation zone, both a consequence of climate warming. This explains the increased frequency of glacier collapse events (Figure 1) and that such events are likely to be a more frequent occurrence at Alpine glacier margins as climate warming continues.

Acknowledgments, Samples, and Data

- This project was funded by the Canton de Vaud. We thank the authorities of the Commune de Bagnes for granting access to the field site. We acknowledge Dr. Andreas Bauder, Dr. Mauro Werder, and Dr. Daniel Farinotti from VAW at ETH Zurich for providing us with the most recent Swiss ice thickness and bed topography datasets.

- No real or perceived financial conflicts of interest are present for this article.
- None of the authors has an affiliation that may present a conflict of interest for this article.
- The data supporting the conclusions meets FAIR principles and is supplied with this paper for the purposes of review under the following link: https://datadryad.org/stash/share/Ig5BhqwviMUgdDaLt-kP3FB_giWPZRBqMC0cvfNzKA4 .

References

Bartholomaus, T. C., Anderson, R. S., & Anderson, S. P. (2011). Growth and collapse of the distributed subglacial hydrologic system of Kennicott Glacier, Alaska, USA, and its effects on basal motion. *Journal of Glaciology*, *57*, 985-1002.

Church, G., Bauder, A., Grab, M., & Maurer, H. (2021). Ground-penetrating radar imaging reveals glacier's drainage network in 3D. *The Cryosphere*, 15, 3975–3988, https://doi.org/10.5194/tc-15-3975-2021

Costa, A., Molnar, P., Stutenbecker, L., Bakker, M., Silva, T. A., Schlunegger, F., ... & Girardclos, S. (2018). Temperature signal in suspended sediment export from an Alpine catchment. *Hydrology and earth system sciences*, *22*, 509-528.

Cuffey, K. M., & Paterson, W. S. B. (2010). *The physics of glaciers*. Academic Press.

Cutler, P. M. (1998). Modelling the evolution of subglacial tunnels due to varying water input. *Journal of Glaciology*, *44*, 485-497.

Dewald, N., Lewington, E. L. M., Livingstone, S. J., Clark, Ch. D. & Storrar, R. D. (2021). Distribution, Characteristics and Formation of Esker Enlargements. Geomorphology, https://doi.org/10.1016/j.geomorph.2021.107919.

Dey, S., & Ali, S. Z. (2017). Origin of the onset of meandering of a straight river. *Proceedings of the Royal Society A: Mathematical, Physical and Engineering Sciences*, *473*, Article number 20170376.

Egli, P., Irving, J., & Lane, S. (2021). Characterization of subglacial marginal channels using 3-D analysis of high-density ground-penetrating radar data. *Journal of Glaciology, 67*, 759-72

Fountain, A. G., & Walder, J. S. (1998). Water flow through temperate glaciers. *Reviews of Geophysics*, *36*, 299-328.

Gantayat, P., Kulkarni, A. V., & Srinivasan, J. (2014). Estimation of ice thickness using surface velocities and slope: case study at Gangotri Glacier, India. *Journal of Glaciology*, *60*, 277-282.

Gindraux, S., Boesch, R., & Farinotti, D. (2017). Accuracy assessment of digital surface models from unmanned aerial vehicles' imagery on glaciers. *Remote Sensing*, *9*, Article number 186.

GLAMOS (1881-2019), The Swiss Glaciers 1880-2016/17, Glaciological Reports No 1-138, Yearbooks of the Cryospheric Commission of the Swiss Academy of Sciences (SCNAT), published since 1964 by VAW / ETH Zurich, doi:10.18752/glrep_series.

Glen, J. W. (1958). The flow law of ice: A discussion of the assumptions made in glacier theory, their experimental foundations and consequences. *IASH Publ*, *47*, e183.

Grab, M., Mattea, E., Bauder, A., Huss, M., Rabenstein, L., Hodel, E., ... & Maurer, H. (2021). Ice thickness distribution of all Swiss glaciers based on extended ground-

penetrating radar data and glaciological modeling. *Journal of Glaciology*, First View: 1-19.

Hooke, R. L. (1984). On the role of mechanical energy in maintaining subglacial water conduits at atmospheric pressure. *Journal of Glaciology*, *30*, 180-187.

Haeberli, W., & Hölzle, M. (1995). Application of inventory data for estimating characteristics of and regional climate-change effects on mountain glaciers: a pilot study with the European Alps. *Annals of Glaciology*, *21*, 206-212.

Hart, J. K. (1995). An investigation of the deforming layer/debris-rich basal-ice continuum, illustrated from three Alaskan glaciers. *Journal of Glaciology*, *41*(139), 619-633.

Huss, M., Jouvet, G., Farinotti, D., & Bauder, A. (2010). Future high-mountain hydrology: a new parameterization of glacier retreat. *Hydrology and Earth System Sciences*, *14*, 815-829.

Hooke, R. L. (1984). On the role of mechanical energy in maintaining subglacial water conduits at atmospheric pressure. *Journal of Glaciology*, *30*, 180-187.

Hooke, R. L., Laumann, T., & Kohler, J. (1990). Subglacial water pressures and the shape of subglacial conduits. *Journal of Glaciology*, *36*, 67-71.

James, M. R., Antoniazza, G., Robson, S., & Lane, S. N. (2020). Mitigating systematic error in topographic models for geomorphic change detection: accuracy, precision and considerations beyond off-nadir imagery. *Earth Surface Processes and Landforms*, *45*, 2251-2271.

James, M. R., Chandler, J. H., Eltner, A., Fraser, C., Miller, P. E., Mills, J. P., ... & Lane, S. N. (2019). Guidelines on the use of structure-from-motion photogrammetry in geomorphic research. *Earth Surface Processes and Landforms*, *44*, 2081-2084.

James, M. R., Robson, S., & Smith, M. W. (2017). 3-D uncertainty-based topographic change detection with structure-from-motion photogrammetry: precision maps for ground control and directly georeferenced surveys. *Earth Surface Processes and Landforms*, *42*, 1769-1788.

Jarque, C.M. and Bera, A.K., 1980. Efficient tests for normality, homoscedasticity and serial independence of regression residuals. *Economics Letters, 6*, 255–259

Jouvet, G., Huss, M., Funk, M., & Blatter, H. (2011). Modelling the retreat of Grosser Aletschgletscher, Switzerland, in a changing climate. *Journal of Glaciology*, *57*, 1033-1045.

Kellerer-Pirklbauer, A., and Kulmer, B. (2019) The evolution of brittle and ductile structures at the surface of a partly debris-covered, rapidly thinning and slowly moving

glacier in 1998–2012 (Pasterze Glacier, Austria), *Earth Surf. Process. Landforms*, 44, 1034– 1049.

Kohler, J. (1995). Determining the extent of pressurized flow beneath Storglaciären, Sweden, using results of tracer experiments and measurements of input and output discharge. *Journal of Glaciology*, *41*, 217-231.

Konrad, S. K. (1998). Possible outburst floods from debris-covered glaciers in the Sierra Nevada, California. *Geografiska Annaler: Series A, Physical Geography*, *80*, 183-192.

Lindström, E (1993) Esker enlargements in Northern Sweden, *Geografiska Annaler: Series A, Physical Geography*, 75, 95-110

Loewe, F. (1957). Subglacial stoping or block caving. *Journal of Glaciology, 3*, 152-152.

Mann, H.B., Whitney, D.R., 1947. On a test of whether one of two Random variables is stochastically larger than the other. *Annals of Mathematical Statistics, 18*, 50–60.

Moore, P. L., Iverson, N. R., & Cohen, D. (2009). Ice flow across a warm-based/cold-based transition at a glacier margin. *Annals of Glaciology*, *50*, 1-8.

Nienow, P., Sharp, M., & Willis, I. (1998). Seasonal changes in the morphology of the subglacial drainage system, Haut Glacier d'Arolla, Switzerland. *Earth Surface Processes and Landforms, 23*, 825-843.

Nye, J. F. (1953). The flow law of ice from measurements in glacier tunnels, laboratory experiments and the Jungfraufirn borehole experiment. *Proceedings of the Royal Society of London. Series A. Mathematical and Physical Sciences*, *219*, 477-489.

Paul, F., Azzoni, R.S., Fugazza, D., Le Bris, R., Nemec, J., Paul, F., Rabatel, A., Ramusovic, M., Rastner, Ph., Schaub, Y., Schwaizer (née Bippus), G. (2019) *GLIMS Glacier Database*. Boulder, CO. National Snow and Ice Data Center. http://dx.doi.org/10.7265/N5V98602

Paul, F., & Haeberli, W. (2008). Spatial variability of glacier elevation changes in the Swiss Alps obtained from two digital elevation models. *Geophysical Research Letters*, *35*, L21502

Paige, R. (1956). Subglacial stoping or block caving: a type of glacier ablation. *Journal of Glaciology, 2*, 727-729.

Rippin, D. M., Pomfret, A., & King, N. (2015). High resolution mapping of supra-glacial drainage pathways reveals link between micro-channel drainage density, surface roughness and surface reflectance. *Earth Surface Processes and Landforms*, *40*, 1279-1290.

Rossini, M., Di Mauro, B., Garzonio, R., Baccolo, G., Cavallini, G., Mattavelli, M.,…, Colombo, R. (2018). Rapid melting dynamics of an alpine glacier with repeated uav photogrammetry. *Geomorphology, 304*, 159-172.

Salzmann, N., Machguth, H., & Linsbauer, A. (2012). The Swiss Alpine glaciers' response to the global '2° C air temperature target'. *Environmental Research Letters*, *7*, 044001.

Shreve, R. L. (1972). Movement of water in glaciers. *Journal of Glaciology*, *11*, 205-214.

Stocker-Waldhuber, M., Fischer, A., Keller, L., Morche, D., & Kuhn, M. (2017). Funnel-shaped surface depressions—indicator or accelerant of rapid glacier disintegration? A case study in the Tyrolean Alps. *Geomorphology*, *287*, 58-72.

SwissTopo (2021), https://map.geo.admin.ch

Westoby, M. J., Brasington, J., Glasser, N. F., Hambrey, M. J., & Reynolds, J. M. (2012). `structure-from-motion' photogrammetry: A low-cost, effective tool for geoscience applications. *Geomorphology, 179*, 300-314.

Zekollari, H., Huss, M., & Farinotti, D. (2019). Modelling the future evolution of glaciers in the European Alps under the EURO-CORDEX RCM ensemble. *The Cryosphere*, *13*, 1125-1146.